Proc. of the European Safety and Reliability Conference (ESREL 2026)
Edited by José C. Matos, Paulo B. Lourenço, Michael Beer, Daniel Oliveira,
Edoardo Patelli, Hélder S. Sousa, Rui A. Silva and Monica Santamaria
 Published by Research Publishing, Singapore.
doi: 10.3850/ESREL2026061419_esrel26-p27792-cd

Multiscale load collective modelling for an electrolyser cell frame under market-driven operation

Dominik Robert Naake
Battolyser Systems, The Netherlands. E-mail: dominik@battolysersystems.com

Arvin Tavanaei
Battolyser Systems, The Netherlands. E-mail: arvin@battolysersystems.com

The increasing penetration of renewable energy in power systems results in highly intermittent operating conditions for power-to-hydrogen assets. Alkaline water electrolysers are traditionally designed for and operated in a base load scenario, i.e. permanently at high load. Consequently, intermittency means that assets are increasingly operated under market-driven dispatch, involving partial-load operation, frequent start-stop events, and idle periods, yielding additional component stress. To support reliable design and assessment of such systems, realistic and traceable methods are required to derive mechanical load collectives for critical components. This paper presents a multiscale modelling framework, quantifying fatigue-relevant load spectra for an electrolyser cell frame, with a particular focus on mechanical loads during idle operation. Long-term operating profiles are generated using a coupled electricity and hydrogen market model that captures price variability, energy availability, and dispatch behaviour. Idle periods are identified and mapped to temperature and pressure cycles due to shutdown, via a reduced physical model. A mechanical model translates these cycles into stress ranges and occurrence counts for the stack cell frame. The resulting load collectives provide a transparent link between market-driven operation and component-level mechanical loading, highlighting the contribution of idle periods to variable-amplitude stress histories, supporting the fatigue-oriented assessment of electrolyser components under flexible operation.

Keywords: Pressurised alkaline water electrolysis, intermittent power profile, mechanical load collective derivation.

1. Introduction

The increasing penetration of renewable energy sources in power systems has been associated with greater short-term variability and volatility in electricity prices and power availability, driven by the intermittency of wind and solar generation and its effects on residual load and market clearing (Cevik and Ninomiya, 2022; Seel et al., 2018). In parallel, hydrogen is increasingly positioned as a cross-sectoral energy carrier, with electrolysis-based power-to-hydrogen assets expected to provide flexibility while enabling sector coupling (International Energy Agency, 2022; Brown, T. and D. Schlachtberger, A. Kies, S. Schramm, and M. Greiner, 2018). Consequently, water electrolysers are increasingly operated under price-driven, time-varying dispatch, characterised by partial-load operation, frequent load ramps, and repeated start–stop cycling with short and extended idle periods (Buttler and Spliethoff, 2018; Schlund and Theile, 2021; Bergen et al., 2009; Zheng et al., 2022). For alkaline systems, these operating trajectories translate into evolving thermodynamic states and associated mechanical loads. Idle periods represent a distinct operating manoeuvre, involving cooling and inherent partial depressurisation phases followed by restart and load re-application. This can produce variable-amplitude stress–time histories with transient load excursions during shutdown and idle-to-load transitions (Bergen et al., 2009). In this work, the focus lies on the polymeric cell frame, carrier for the electrode assembly, the electrochemical building blocks of the electrolyser.

Most studies addressing electrolyser flexibility adopt a system-level perspective, emphasising techno-economic metrics such as efficiency, hydrogen production cost, optimal dispatch, and grid integration or ancillary service provision (Glenk and Reichelstein, 2019). These approaches rarely link variable operating profiles to component-

level mechanical loading. Conversely, mechanical and structural analyses typically rely on prescribed representative operating profiles, duty cycles, or envelope load cases (European Commission Joint Research Centre, 2023), which may not capture irregular sequences, in particular the frequency, duration, and sequencing of idle periods under market-driven dispatch. More fundamentally, little is known about the dynamic load profiles experienced by (especially alkaline) electrolyser components under realistic, market-driven operation, especially the transient evolution of internal stresses due to consequences of dynamic load profiles. The literature therefore concentrates either on techno-economic optimisation and system integration, or on the electrochemical degradation of active cell components under dynamic electrical loading (Pape et al., 2025; Maoulida et al., 2025; Wallnöfer-Ogris et al., 2024), while studies that derive mechanical load collectives from realistic operating histories and relate them to structural fatigue-relevant stress spectra remain largely absent. Fatigue damage accumulation is material-dependent and sensitive to variable-amplitude loading and the statistical characteristics of stress cycles, motivating representative load collectives derived from realistic operating profiles (Schijve, 2009; International Organization for Standardization, 2012). For polymeric components, viscoelasticity, mean stress sensitivity, and load–time characteristics govern fatigue behaviour across the low- to high-cycle regime (Kausch, 1987; Hertzberg et al., 2013; ASTM International, 2021). Idle operation can therefore influence stress amplitudes and cycle distributions, motivating the extraction of stress cycles and spectra from operational histories.

Against this background, this paper presents a multiscale modelling framework with the goal of linking market-driven electrolyser operation to mechanical load collectives for the electrolyser cell frame, with emphasis on quantifying idle operation and its contribution to fatigue-relevant mechanical loading.

2. Multiscale modelling framework overview

The proposed framework establishes a transparent and traceable workflow linking market-driven electrolyser operation to component-level mechanical loading, with a focus on the cell frame of an electrolyser stack. Owing to the limited availability of measurement data for dynamically operated alkaline water electrolysers due to the novelty of pronounced dynamic usage, the mechanical loading behaviour is derived using a model-based approach. Figure 1 shows a simplified representation of the electrolyser system considered in this work, including the stack, separators, piping, and power supply. Balance-of-plant components beyond this scope are neglected.

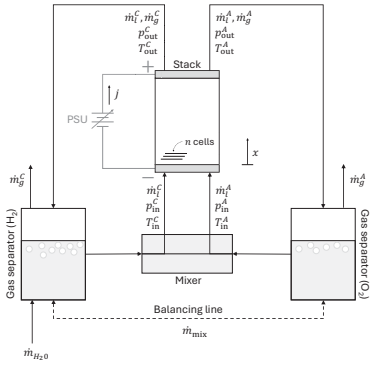

Fig. 1. Simplified electrolyser plant layout considered in this study.

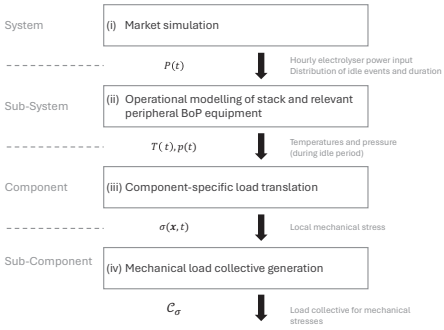

Fig. 2. Multiscale modelling framework linking market-driven operation to mechanical load collectives.

The modelling framework follows a top-down structure (cf. fig. 2), starting from a coupled electricity and hydrogen market model that generates long-term operating profiles. These are transferred to a reduced physical model to evaluate thermal and pressure dynamics during idle periods. Subsequently, a component-level mechanical model translates these dynamics into local stress states. The resulting stress–time histories are post-processed to derive fatigue-relevant load collectives.

3. Market-driven system-level operation modelling

3.1. *Coupled electricity and hydrogen market model*

The internally developed system level techno-economical model (TEM) represents the interaction between electricity markets, renewable generation, and hydrogen production (Połchłopek et al., 2024). Prices in various electricity sources i.e. Power Purchase Agreements (*PPA*) from renewable sources and spot markets, like Day-ahead (*DA*), Intraday (*ID*), and Imbalance (*IM*), covering intermittency and daily/seasonal variability. Data was obtained under license from a commercial energy market data provider, providing forecasts for the wholesale electricity markets (Montel Group Ltd., 2024). Figure 3 shows an example of the TEM input data in a 48-hour period.

Hydrogen production is assumed to respond to electricity price signals, subject to technical constraints of the electrolyser and the grid. Depending on the market scenario, hydrogen demand may be fixed or price-driven, influencing the dispatch behaviour of the system.

3.2. *Electrolyser dispatch and operating behaviour*

The electrolyser is operated according to an economically motivated dispatch strategy that allocates available electricity resources to hydrogen production under market conditions. Dispatch decisions are driven by electricity procurement costs, contractual commitments, and technical operating constraints, with the objective of maximising the economic value of operation. Revenues are generated through the sale of hydrogen, including hydrogen qualifying under applicable regulatory frameworks for green hydrogen (e.g. RFNBO), and may be supplemented by electricity market arbitrage revenues enabled by flexible electrolyser operation. Operational expenditures include electricity procurement, labour, maintenance, and repair costs. Technical constraints such as minimum and maximum operating load and power-dependent conversion efficiency derived from electrode polarisation characteristics, are considered.

The operational profile is determined via rolling-horizon optimisation at an hourly resolution, with fixed daily decision epochs corresponding to market gate closure. The optimisation accounts for multiple electricity procurement channels, cf. section 3.1. At each decision epoch $d \in \mathcal{D}$, an optimisation problem is solved over a finite look-ahead horizon $\mathcal{H}_d = \{d, \ldots, d + H - 1\}$:

$$\max_{\{P_t\}_{t\in\mathcal{H}_d}} \quad \sum_{t\in\mathcal{H}_d} \beta_t \left(R_t(P_t) - C_t(P_t)\right), \qquad (1)$$

where H denotes the length of the look-ahead (prediction) horizon, $\beta_t = (1+r)^{-\tau(t)}$ is the discount factor with discount rate r, $R_t(P_t)$ denotes the revenue associated with hydrogen production

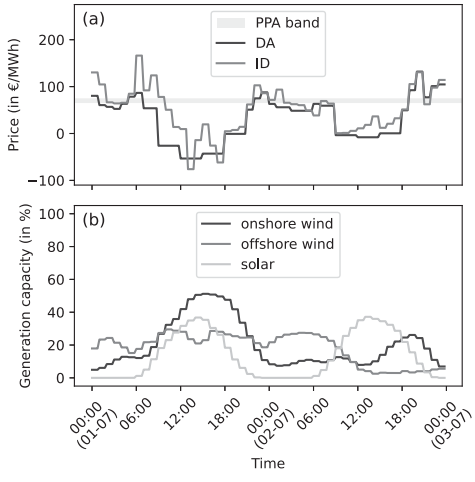

Fig. 3. Representative forecast data of selected electricity markets (*DA* and *ID*) and nominal renewable generation capacity (wind and solar) for July 1 and 2, 2030 in the Netherlands.

and potential electricity market arbitrage at time step t, and $C_t(P_t)$ the corresponding operational cost.

The optimisation is subject to the constraints

$$\begin{aligned} P_t \in \{0\} \cup [P_{\min}, P_{\max}] \qquad & \forall t \in \mathcal{H}_d, \\ P_t = P_t^{\mathrm{M}} \qquad & \forall t \in \mathcal{C}_d. \end{aligned} \tag{2}$$

Here, P_t denotes the hourly electrolyser power input. The admissible operating set $\{0\} \cup [P_{\min}, P_{\max}]$ represents two operating modes: shutdown or idle operation ($P_t = 0$) and power operation within the admissible partial-load range ($P_{\min} \leq P_t \leq P_{\max}$). The variable P_t^{M} denotes the power schedule committed via the selected market mechanism (*PPA*, *DA*, or *ID*) for the corresponding delivery period $\mathcal{C}_d \subseteq \mathcal{H}_d$.

The primary engineering-relevant outputs of the system-level model are long-term time series of electrical power input, here in an hourly resolution. Figure 4 illustrates an excerpt of the resulting operating profile for a two-day window within a typical fifteen-year use-case simulation. The electrolyser operates across a wide range of partial-load conditions, as shown in fig. 5a, and experiences frequent transitions between operating states, illustrated by the dynamic load heatmap in fig. 5b. With focus on the effects of idle operation, an analysis of idle period occurences and their respective duration is performed. The results are depicted in fig. 5c. The resulting histogram indicates that idle operation is dominated by short-duration events, while longer idle periods occur less frequently but remain non-negligible, reflecting a highly intermittent operating pattern.

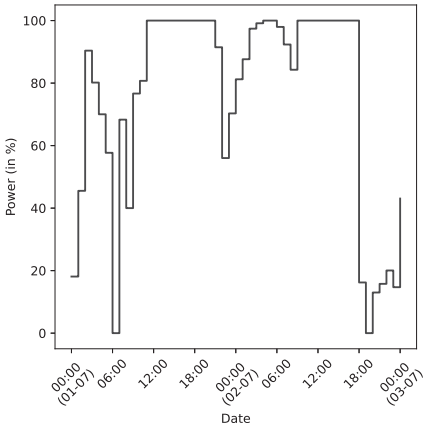

Fig. 4. Techno-economical model output. Example data for a 48-hour period (July 1 and 2, 2030).

4. Transfer from system operation to electrolyser load inputs

To transfer system-level operation to physically meaningful electrolyser load inputs, a reduced representation of the electrolyser is adopted. The objective is to capture the dominant thermal dynamics relevant during idle periods while avoid-

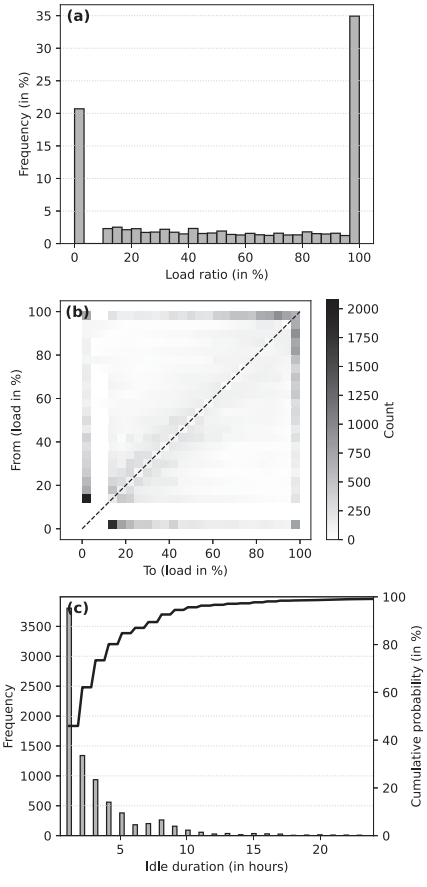

Fig. 5. Postprocessed TEM results for a use-case with 15-year duration: (a) Distribution of loads over the partial load range and idle, (b) heat map of dynamic load changes, and (c) event count per of idle duration $t_j \in [0, 24]$ h of class j.

ing unnecessary model complexity. The following simplifying assumptions are therefore introduced:

(1) The analysis is restricted to the electrolyser system as depicted in fig. 1, i.e. stack, separators and piping. Other Balance-of-plant components are neglected.
(2) The stack temperature is assumed to be spatially uniform and actively controlled ($\Delta T = (T_{\mathrm{out}} - T_{\mathrm{in}}) \approx \text{const.}$) during operation. Consequently, no temperature gradients within the stack are considered, and no temperature deviations due to partial-load operation are expected. We assume a mean temperature T_0 as representative.
(3) System pressure is assumed to be ideally regulated during partial and full load operation. Pressure variations due to changing flow rates, pressure losses in channels or manifolds, and anode–cathode pressure differentials are neglected.

Under these assumptions, temperature dynamics are only relevant during idle periods in which the stack cools down passively. The problem therefore reduces to the description of the system cooling curve during idle operation.

The temperature evolution of the electrolyser during idle operation is described using a reduced form of the dynamic thermal model proposed by Brauns and Turek (2023). In this model, the electrolyser is represented by a lumped thermal capacitance C_{sys} and a single, spatially uniform system temperature $T(t)$.

Starting from the general energy balance

$$C_{\mathrm{sys}} \frac{\mathrm{d}T}{\mathrm{d}t} = \dot{Q}_{\mathrm{el}} - \dot{Q}_{\mathrm{loss}} + \dot{Q}_{\mathrm{hc}}, \tag{3}$$

idle operation is defined by an applied current density $j = 0$, such that the electrochemical heat generation term $\dot{Q}_{\mathrm{el}}$ vanishes. For further simplicity, no active heating or cooling is considered during the idle period, i.e. $\dot{Q}_{\mathrm{hc}} = 0$. Under these conditions, the temperature dynamics reduce to

$$C_{\mathrm{sys}} \frac{\mathrm{d}T}{\mathrm{d}t} = -\dot{Q}_{\mathrm{loss}}. \tag{4}$$

Following the heat-loss formulation used by Brauns and Turek, thermal losses to the environment are modeled by natural convection as

$$\dot{Q}_{\mathrm{loss}} = \alpha A_{\mathrm{sys}} \left(T - T_{\mathrm{a}}\right), \tag{5}$$

where α is the effective heat transfer coefficient, A_{sys} the external heat transfer area, and T_{a} the ambient temperature. Substitution yields a first-order linear ordinary differential equation,

$$\frac{\mathrm{d}T}{\mathrm{d}t} = -\frac{\alpha A_{\mathrm{sys}}}{C_{\mathrm{sys}}} \left(T - T_{\mathrm{a}}\right), \tag{6}$$

which admits an analytical solution for constant ambient temperature. For an initial (i.e. nominal) temperature $T_0 = T_{\mathrm{nom}}$ at the beginning of the idle period $t = t_0$, the system temperature after an idle time t_j of class j is given by

$$T(t_0 + t_j) = T_{\mathrm{a}} + (T_0 - T_{\mathrm{a}}) \exp\left(-\frac{\alpha A_{\mathrm{sys}}}{C_{\mathrm{sys}}} t_j\right). \tag{7}$$

Brauns and Turek treat the system pressure as a prescribed constant, i.e. pressure drop due to cool down is neglected in their proposed model. However, here we consider the reactor operated under the assumptions of a closed system (no mass exchange with the surroundings), a rigid volume, and ideal gas behavior in the gas phase. Furthermore, phase change, gas dissolution, and chemical reactions are neglected. Under these conditions, the gas pressure in the headspace is governed by the ideal gas law, $pV = nRT$. Since the amount of gas n and the gas volume V remain constant, the pressure is directly proportional to the absolute temperature. Consequently, when the reactor is idled for time t_j and cools from its nominal operating temperature T_0 to a lower temperature $T(t_j) = T_j < T_0$, the corresponding pressure is given by

$$p(t_j) = p_0 \cdot \frac{T(t_j)}{T_0}. \tag{8}$$

Under the stated assumptions, cooling of the reactor during idle operation leads to a proportional reduction in internal pressure, $p(t_j) = p_j < p_0$.

The model results are depicted in fig. 6, where both temperature and pressure reduce over idle time. The used input parameters are stated in table 1. Under the assumption that the stack temperature is actively controlled to a constant nominal value T_0 during all operating states, the initial

Table 1. Inputs for the idle cool-down model derived from the Brauns temperature submodel and extended by ideal gas pressure loss.

Parameter	Value
Nominal system temperature T_0	273.15 + 80 K
Ambient temperature T_a	273.15 + 20 K
Nominal system pressure p_0	11 bara
Applied current density j (idle)	0 A/cm^{-2}
System thermal capacitance C_sys	50×10^6 J K^{-1}
Heat transfer coefficient α	10 W m^{-2} K^{-1}
External surface area stack A_stack	88 m^2
Uninsulated surface area A_ni	50 m^2

temperature for each idle event is identical. In addition, the heat-up phase following an idle period is assumed to be significantly faster than the cool-down phase, such that the stack can be considered to return to T_0 before the next operating cycle begins. Consequently, every idle period is represented by a similar thermal/pressure cycle $(T_0, p_0) \rightarrow (T_j, p_j) \rightarrow (T_0, p_0)$, where the minimum temperature reached during the idle phase depends solely on the idle duration t_j. For fixed ambient conditions, the resulting temperature and pressure changes per cycle,

$$\begin{aligned} \Delta T(t_j) &= T_j - T_0, \\ \Delta p(t_j) &= p_j - p_0, \end{aligned} \tag{9}$$

are therefore unique functions of the idle time. As a result, the idle-duration histogram can be mapped directly to a distribution of coupled $(\Delta T_j, \Delta p_j)$ cycles with corresponding occurrence counts for each idle duration class j,

$$\{N_j,\ \Delta T_j,\ \Delta p_j\}\,. \tag{10}$$

This direct coupling remains valid as long as the ambient temperature is approximately constant and the system is reheated to T_0 between successive idle events.

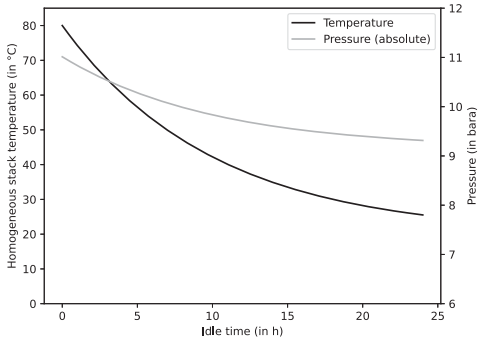

Fig. 6. Idle cool-down of the electrolyser stack following shutdown for the first 24 hours.

5. Mechanical modelling of the electrolyser frame

The thermal and pressure cycles derived from the operational analysis in eq. (10) are translated into mechanical load cycles acting on the electrolyser cell frame. The cell frame is part of a preloaded stack assembly consisting of (steel) end flanges, a series of repeating (mainly polymeric) cell frames, and stud bolts providing the clamping force. As a result, the frame experiences a superposition of stresses originating from bolt preload, internal pressure, and thermally induced deformation.

To efficiently evaluate the large number of operational cycles, a linearized mechanical response model is employed. The mechanical behavior is linearized about the nominal operating state, defined by the nominal temperature T_0, nominal pressure p_0, and the applied bolt preload. This state represents the initial stress condition $\boldsymbol{\sigma}_0$ during operation and serves as the reference configuration for subsequent load perturbations.

The local von Mises stress response σ_vM at a given location A of the cell frame can be approximated by a first-order expansion,

$$\begin{aligned} \sigma_{\mathrm{vM},j} &\approx \sigma_{\mathrm{vM},0} + \Delta\sigma_{\mathrm{vM},j}, \\ &= \sigma_{\mathrm{vM},0} + S_T\,\Delta T_j + S_p\,\Delta p_j \end{aligned} \tag{11}$$

for each idle period of class j in eq. (10), where $\sigma_{\mathrm{vM},0}$ denotes the von Mises stress at nominal operating conditions, $S_T = \partial\sigma_\mathrm{vM}/\partial T$ and $S_p = \partial\sigma_\mathrm{vM}/\partial p$ are the stress sensitivities with respect to temperature and pressure, respectively. The influence of temperature and pressure variations on local stresses is quantified using unit load cases. Two independent finite-element analysis (FEA) are performed at nominal state: (i) a thermal unit load case with a uniform temperature decrease of $\Delta T_\mathrm{u} = -1\,\mathrm{K}$ at constant pressure, and (ii) a

pressure unit load case with a pressure decrease of $\Delta p_{\mathrm{u}} = -0.1\,\mathrm{MPa}$ at constant temperature. From these simulations, stress sensitivities with respect to temperature and pressure are obtained at relevant locations of the cell frame. Table 2 summarises the results of the FEA at a given location A of the cell frame.

Table 2. FEA results of the mechanical stress analysis at a chosen location A.

Result entity	Value
$\sigma_{\mathrm{vM},0}$	13.87 MPa
S_T	0.085 MPa K^{-1}
S_p	0.109 MPa bar^{-1}

6. Derivation of mechanical stress load collective for cell frame hotspot

Each idle event is assumed to form a closed mechanical cycle between nominal operation and the idle minimum, $\sigma_{\mathrm{vM},0} \rightarrow \sigma_{\mathrm{vM},j} \rightarrow \sigma_{\mathrm{vM},0}$, resulting in a von Mises stress range

$$\Delta\sigma_j = \left|\sigma_{\mathrm{vM},j} - \sigma_{\mathrm{vM},0}\right|. \tag{12}$$

The corresponding stress amplitude is given by $\sigma_{\mathrm{a},j} = \Delta\sigma_j/2$. The lower and upper stresses of the cycle are $\sigma_{\mathrm{l},j} = \min(\sigma_{\mathrm{vM},0}, \sigma_{\mathrm{vM},j})$ and $\sigma_{\mathrm{u},j} = \max(\sigma_{\mathrm{vM},0}, \sigma_{\mathrm{vM},j})$, respectively, yielding a mean stress $\sigma_{\mathrm{m},j} = (\sigma_{\mathrm{l},j} + \sigma_{\mathrm{u},j})/2$, and a load ratio $R_j = \sigma_{\mathrm{l},j}/\sigma_{\mathrm{u},j}$.

The idle-duration histogram (cf. fig. 5c and eq. (10)) provides the occurrence count N_j for each class j. Consequently, the operational history is mapped to a discrete stress-cycle collective of the form

$$\{N_j,\ \Delta\sigma_j,\ \sigma_{\mathrm{a},j},\ \sigma_{\mathrm{m},j},\ R_j\}_A, \tag{13}$$

which constitutes the complete mechanical load collective for the considered hotspot A. The discrete stress cycles are represented as a load collective, in which the untransformed (in R) stress range $\Delta\sigma$ is plotted as a function of the cumulative number of cycles N, cf. fig. 7. It provides a compact representation of the stress spectrum and highlights the relative contribution of rare high-load events and more frequent low-load cycles.

7. Conclusion

The proposed workflow establishes a link between market-driven dispatch and fatigue-relevant mechanical loading of the electrolyser cell frame. It enables systematic construction of mechanical load collectives derived from operating histories with focus on idle operation. Long-term operating profiles generated by a coupled electricity and hydrogen market model were analysed. Idle events allocate a substantial share ($\approx 20\%$) of the electrolysers service time, distributed over a broad range of idle durations. These events yield inherent thermal and pressure cycles which are predicted using a reduced physical shutdown model and are translated into component-level stress cycles via a linearised mechanical response model. The results show that idle operations introduce an additional distinct class of load cycles associated with stack cool-down and depressurisation, leading to variable-amplitude stress cycles. These are not captured by conventional steady or partial-load duty assumptions, but have an impact on the component and therefore system reliability. The derived load collective provides a suitable basis for fatigue and reliability analyses for the cell frame component in particular. The proposed

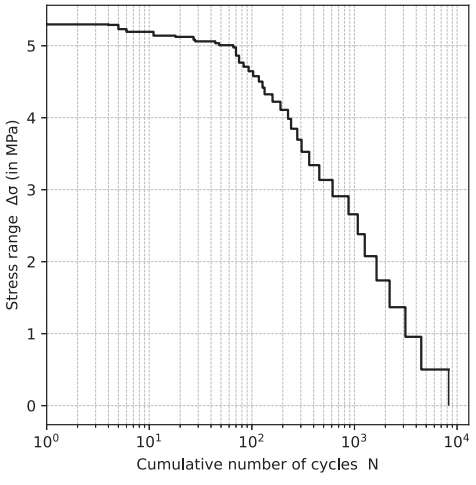

Fig. 7. Load spectrum of the electrolyser cell frame at location A, expressed in terms of the von Mises stress range $\Delta\sigma$ according to eq. (13).

method can be easily adopted for other electrolyser components under flexible operation.

References

ASTM International (2021). ASTM D7791–standard test method for uniaxial fatigue properties of plastics.

Bergen, A., L. Pitt, A. Rowe, P. Wild, and N. Djilali (2009). Transient electrolyser response in a renewable-regenerative energy system. *International Journal of Hydrogen Energy*.

Brauns, J. and T. Turek (2023). Model-based analysis and optimization of pressurized alkaline water electrolysis powered by renewable energy. *Journal of The Electrochemical Society 170*(6).

Brown, T. and D. Schlachtberger, A. Kies, S. Schramm, and M. Greiner (2018). Synergies of sector coupling and transmission reinforcement in a cost-optimised, highly renewable european energy system. *Energy 160*, 720–739.

Buttler, A. and H. Spliethoff (2018). Current status of water electrolysis for energy storage, grid balancing and sector coupling via power-to-gas and power-to-liquids: A review. *Renewable and Sustainable Energy Reviews 82*, 2440–2454.

Cevik, S. and K. Ninomiya (2022). Energy transition and electricity prices in europe. Technical Report No. 2022/220, International Monetary Fund.

European Commission Joint Research Centre (2023). Harmonised testing protocols for water electrolysers.

Glenk, G. and S. Reichelstein (2019). Economics of converting renewable power to hydrogen. *Nature Energy 4*, 216–222.

Hertzberg, R. W., R. P. Vinci, and J. L. Hertzberg (2013). *Deformation and Fracture Mechanics of Engineering Materials* (5th ed.). Hoboken, NJ: Wiley.

International Energy Agency (2022). Global hydrogen review 2022.

International Organization for Standardization (2012). ISO 12107:2012–Metallic materials–Fatigue testing–Statistical planning and analysis of data.

Kausch, H. H. (1987). *Fatigue of Polymers*. Berlin: Springer.

Maoulida, F., D. Guilbert, M.-B. Camara, and B. Dakyo (2025). Dynamic electrical degradation of PEM electrolyzers under renewable energy intermittency: mechanisms, diagnostics, and mitigation strategies. *Renewable and Sustainable Energy Reviews 185*.

Montel Group Ltd. (2024). Energy market price, renewable generation, and offtake data. Accessed under commercial licence.

Pape, S.-V., S. Zerressen, M. F. Seidler, R. Keller, F. Lohmann-Richters, M. Müller, U.-P. Apfel, A. K. Mechler, and A. Glüsen (2025). Dynamic operation and degradation of alkaline water electrolysis cells under renewable energy profiles. *International Journal of Hydrogen Energy 127*, 51–63.

Połchłopek, O., S. de Haas, and G. Massabie (2024). Balancing act: the impact of electrolyser flexibility on green hydrogen cost, industry decarbonization and system integration. Technical report, Battolyser Systems.

Schijve, J. (2009). *Fatigue of Structures and Materials*. Dordrecht: Springer.

Schlund, D. and P. Theile (2021). Simultaneity of green energy and hydrogen production: Analysing the dispatch of a grid-connected electrolyser. Technical Report No. 21/10, Institute of Energy Economics at the University of Cologne (EWI).

Seel, J., A. D. Mills, R. H. Wiser, S. Deb, A. Asokkumar, M. Hassanzadeh, and A. Aarabali (2018). Impacts of High Variable Renewable Energy Futures on Wholesale Electricity Prices, and on Electric-Sector Decision Making. Technical Report 1437006, Lawrence Berkeley National Laboratory.

Wallnöfer-Ogris, E., M. Böhm, and V. Hacker (2024). Understanding and identifying degradation mechanisms in PEM water electrolysis cells: A review. *International Journal of Hydrogen Energy 49*(15), 12234–12258.

Zheng, Y., S. You, H. W. Bindner, and M. Münster (2022). Optimal day-ahead dispatch of an alkaline electrolyser system concerning thermal–electric properties and state-transitional dynamics. *Applied Energy 307*.